

## Chapter 4

### A TOOL FOR INVERSE MODELING OF SPECTRAL MEASUREMENTS IN DEEP AND SHALLOW WATERS

PETER GEGE<sup>1</sup> AND ANDREAS ALBERT<sup>2</sup>

<sup>1</sup>*DLR, Remote Sensing Technology Institute, P.O.Box 1116, 82230 Wessling, Germany*

<sup>2</sup>*GSF, Institute of Soil Ecology, Ingolstaedter Landstr. 1, 85764 Neuherberg, Germany*

*Email: peter.gege@dlr.de, andreas.albert@gsf.de*

#### 1. Introduction

Light is the primary energy source of life on Earth. Apart from some deep-sea ecosystems, the existence of all organisms depends directly or indirectly on the process of photosynthesis, which is driven by electromagnetic radiation in the spectral range from 400 to 700 nm (photosynthetically active radiation, or PAR), or at longer wavelengths for some photosynthetic bacteria. Solar irradiance and the transparency of water are maximal, and atmospheric extinction is low, at PAR wavelengths. Thus, optical in this spectral range can provide valuable information to characterize biological processes in aquatic ecosystems.

Many different types of optical instruments have been developed which can be used to quantitatively determine certain parameters of aquatic ecosystems. These instruments are operated on buoy, off shore platforms, ships, aircraft, and satellites, and measure radiation in different spectral bands. Remote sensing instruments usually provide images, thus measuring *radiance spectra* of individual pixels. *In situ* optical instruments can measure radiation with angle-integration (irradiance), with normalization to incident illumination (reflectance), with alterations versus depth (attenuation), or the fractions which are absorbed, scattered, or emitted in the water or from the dissolved or suspended constituents.

Usually data from each instrument, or sensor type, are analyzed with software that is specifically tailored to that instrument or spectrum. However, operating a group of programs is a potential source of errors, because the data analysis programs must be consistent with each other with respect to the model formulations and input data. In addition, maintenance and data handling are time consuming, as is training new staff. For these reasons it is desirable to have a single integrative program. Such a tool, the "Water colour Simulator" WASI, was developed for optical *in situ* measurements. The program, together with a detailed user manual, is provided on the CD-ROM accompanying this book. It can also be downloaded from an ftp server (Gege, 2002a).

WASI is designed as a sensor-independent spectra generator and spectra analyzer. The program has well documented calculation steps and automated, graphical visualization of results. It can also generate and analyze large series of spectra. In the forward mode, up to three parameters can be iterated simultaneously to produce a great variety of spectra, while in the inverse mode an unlimited number of spectra can be read from files and automatically analyzed. The supported spectrum types are listed in Table 1. Calculations are based on analytical models. The data provided with WASI were determined at Lake Constance (Gege, 1994, 1995; Heege, 2000) and are suited for calculating all spectral types at a range of at least 390 to 800 nm and with 1 nm spectral resolution.

**Table 1.** Types of spectral measurements for which inverse modeling is implemented.

<b>Spectrum type</b>	<b>Model options</b>	<b>Symbol</b>	<b>Equation</b>
Absorption	Exclude pure water	$a_{WC}(\lambda)$	(1)
	Include pure water	$a(\lambda)$	(3)
Attenuation	For downwelling irradiance	$K_d(\lambda)$	(5)
Specular reflectance	Wavelength dependent	$R_{rs}^{surf}(\lambda)$	(13a)
	Constant	$R_{rs}^{surf}$	(13b)
Irradiance reflectance	For deep water	$R(\lambda)$	(14)
	For shallow water	$R^{sh}(\lambda)$	(16)
Remote sensing reflectance	Below surface for deep water	$R_{rs}^{-}(\lambda)$	(17)
	Below surface for shallow water	$R_{rs}^{sh-}(\lambda)$	(19)
	Above surface	$R_{rs}(\lambda)$	(20)
Bottom reflectance	For irradiance sensors	$R^b(\lambda)$	(21)
	For radiance sensors	$R_{rs}^b(\lambda)$	(22)
Downwelling irradiance	Above surface	$E_d(\lambda)$	(23)
	Below surface	$E_d^{-}(\lambda)$	(24)
Upwelling radiance	Below surface	$L_u^{-}(\lambda)$	(26)
	Above surface	$L_u(\lambda)$	(27)

All input and output files in WASI are in text format (ASCII), making it easy to adapt calculations to regional circumstances by replacing some default input spectra and changing material-specific constants. A well-designed graphical user interface allows intuitive operation. An example of the interface is shown in Figure 1. Alternatively, WASI can be operated in a background mode where all actions are controlled by an input file. In this mode other programs can utilize WASI as a slave to generate or analyze data according to their demands. This input file, WASI.INI, is also used to initialize and document all program settings. It is automatically read during program start up, and a copy with the actual settings is automatically stored in the relevant directory whenever outputs from calculations are saved.

An overall description of WASI was given in Gege (2004). This chapter focuses on data analysis for inverse modeling of spectral measurements. Implemented algorithms, including newly developed models for shallow water, are summarized. Problems associated with inverse modeling, and solutions offered for WASI, are discussed. Finally, some examples of how to apply the program effectively are presented.

## 2. Models

### 2.1 ABSORPTION

#### 2.1.1 Water constituents

Absorption of a mixture of water constituents is the sum of the components' absorption coefficients:

$$a_{WC}(\lambda) = \sum_{i=0}^5 C_i \cdot a_i^*(\lambda) + X \cdot a_X^*(\lambda) + Y \cdot a_Y^*(\lambda), \quad (1)$$

where  $\lambda$  denotes wavelength. Three groups of water absorbing constituents are considered: phytoplankton, non-chlorophyllous particles, and Gelbstoff.

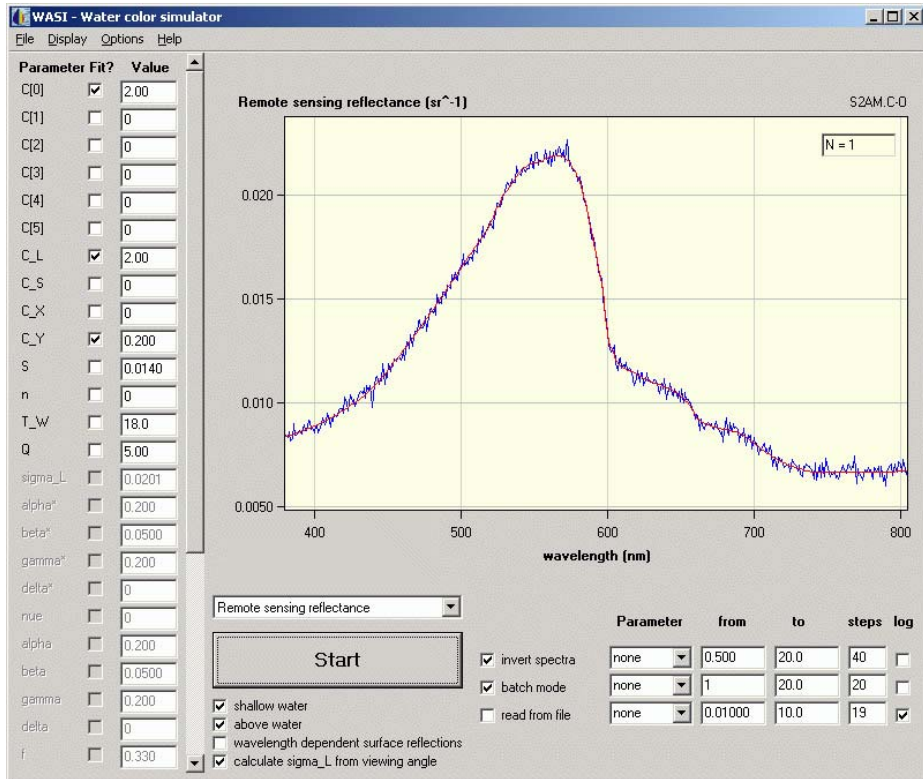


Figure 1. Graphical user interface of WASI in the inverse mode.

*Phytoplankton.* The high number of species that occur in natural waters causes variability in phytoplankton absorption properties. This is accounted for by the inclusion of 6 specific absorption spectra,  $a_i^*(\lambda)$ . If no phytoplankton classification is performed, the spectrum  $a_0^*(\lambda)$  is selected to represent the specific absorption of phytoplankton.  $C_i$  indicates pigment concentration, where “pigment” is the sum of chlorophyll *a* and phaeophytin *a*.

The default spectra provided with WASI are based on measurements at Lake Constance. The five spectra  $a_1^*(\lambda)$ ... $a_5^*(\lambda)$  represent the lake’s major optical classes “cryptophyta type L”, “cryptophyta type H”, “diatoms”, “dinoflagellates”, and “green algae” (Gege, 1994, 1995, 1998b). The spectrum  $a_0^*(\lambda)$  is a weighted sum of these five spectra and represents a mixture which can be considered as typical for that lake. This was calculated by Heege (2000) using in-situ spectra of phytoplankton absorption which were derived from reflectance measurements (Gege, 1994, 1995) and pigment data from 32 days in 1990 and 1991. The spectrum  $a_0^*(\lambda)$  was validated (by Heege) using 139 irradiance reflectance and 278 attenuation measurements from 1990 to 1996.

*Non-chlorophyllous particles.* Absorption is calculated as the product of concentration  $X$  and specific absorption  $a_X^*(\lambda)$ . The spectrum  $a_X^*(\lambda)$  provided with WASI is taken from Prieur and Sathyendranath (1981). It is normalized to 1 at a reference wavelength  $\lambda_0$  of 440 nm.

*Gelbstoff (dissolved organic matter).* Gelbstoff absorption is the product of concentration  $Y$  and specific absorption  $a_Y^*(\lambda)$ . The spectrum  $a_Y^*(\lambda)$  can either be read from file or calculated using the following exponential approximation (Nyquist, 1979; Bricaud et al., 1981):

$$a_Y^*(\lambda) = \exp[-S \cdot (\lambda - \lambda_0)], \quad (2)$$

where  $S$  denotes the spectral slope, and  $\lambda_0$  is a reference wavelength with  $a_Y^*$  normalized to 1. Default values are  $\lambda_0 = 440$  nm and  $S = 0.014$  nm<sup>-1</sup>, which are representative of many types (Bricaud et al., 1981; Carder et al., 1989).

### 2.1.2 Natural water

The bulk absorption of a natural water body is the sum of absorption of pure water and of the water constituents:

$$a(\lambda) = a_w(\lambda) + (T - T_0) \cdot \frac{da_w(\lambda)}{dT} + a_{wc}(\lambda). \quad (3)$$

Absorption of pure water is defined by a temperature-independent term  $a_w$ , which is valid for a reference temperature  $T_0$ , and a temperature gradient  $da_w/dT$  with  $T$  being the actual water temperature. For  $a_w(\lambda)$ , the spectrum measured by Buiteveld et al. (1994) at  $T_0 = 20^\circ\text{C}$  is used for a spectral range of 391–787 nm. For  $da_w/dT$  a spectrum measured by one of the authors (Gege, unpublished data) is used.

## 2.2 BACKSCATTERING

Backscattering ( $b_b$ ) of a water body is the sum of backscattering by pure water ( $W$ ) and suspended matter. For the latter, a distinction between large ( $\geq 5$   $\mu\text{m}$ ,  $L$ ) and small ( $\leq 5$   $\mu\text{m}$ ,  $S$ ) particles is made. Thus, the following parameterization is chosen:

$$b_b(\lambda) = b_{b,w}(\lambda) + C_L \cdot b_{b,L}^* \cdot b_L(\lambda) + C_S \cdot b_{b,S}^* \cdot (\lambda/\lambda_S)^n. \quad (4)$$

### 2.2.1 Pure water

For pure water, the empirical relation of Morel (1974) is used:  $b_{b,w}(\lambda) = b_1 \cdot (\lambda/\lambda_1)^{-4.32}$ . The specific backscattering coefficient,  $b_1$ , depends on salinity. It is  $b_1 = 0.00111$  m<sup>-1</sup> for fresh water and  $b_1 = 0.00144$  m<sup>-1</sup> for oceanic water with a salinity of 35–38 ‰ with  $\lambda_1 = 500$  nm as the reference wavelength.

### 2.2.2 Large particles

Backscattering by large particles is calculated as the product of concentration  $C_L$ , specific backscattering coefficient  $b_{b,L}^*$ , and normalized scattering function  $b_L(\lambda)$ . The user has several options for calculation:

- $C_L$  can be treated either as an independent parameter, or  $C_L = C_0$  can be assigned, where  $C_0$  is the concentration of phytoplankton class no. 0 (see eq. 1). The latter is useful for Case 1 water types where the concentrations of particles and phytoplankton are highly correlated.
- $b_{b,L}^*$  can be treated either as a constant with a default value of  $0.0086 \text{ m}^2 \text{ g}^{-1}$  (Heege, 2000), or as  $b_{b,L}^* = A \cdot C_L^B$ . Such a non-linear dependency of scattering on concentration was observed for phytoplankton (Morel, 1980). It may be used for Case 1 water types, while  $b_{b,L}^* = \text{constant}$  is appropriate for Case 2 waters with significant sources of non-phytoplankton suspended matter. Typical values of the empirical constants are  $A = 0.0006 \text{ m}^2 \text{ g}^{-1}$  and  $B = -0.37$  (Sathyendranath et al., 1989).
- $b_L(\lambda)$  can either be read from file, or it can be calculated as  $b_L(\lambda) = a_0^*(\lambda_L) / a_0^*(\lambda)$ , where  $a_0^*(\lambda)$  is the specific absorption spectrum of phytoplankton class no. 0 (see eq. 1), and  $\lambda_L$  denotes a reference wavelength. This method assumes that backscattering by large particles originates mainly from phytoplankton cells, and couples absorption and scattering according to the Case 1 waters model of Sathyendranath et al. (1989). However, such coupling may be used in exceptional cases only, since living algae have a negligible influence on the backscattering process by oceanic waters (Ahn et al., 1992), and in Case 2 waters particle scattering is weakly related to phytoplankton absorption in general. In WASI,  $b_L(\lambda) = 1$  is set as default.

### 2.2.3 Small particles

Backscattering by small particles is calculated as the product of concentration  $C_S$ , specific backscattering coefficient  $b_{b,S}^*$ , and a normalized scattering function  $(\lambda/\lambda_S)^n$ . The exponent  $n$ , which determines the spectral shape, depends on particle size distribution. The variable “ $n$ ” is typically about  $-1$  (Sathyendranath et al., 1989) and  $b_{b,S}^*$  is about  $0.005 \text{ m}^2 \text{ g}^{-1}$  for  $\lambda_S = 500 \text{ nm}$ .

## 2.3 ATTENUATION

The diffuse attenuation coefficient of irradiance  $E$  is defined as  $K = -(1/E) dE/dz$ , where  $z$  is the depth. Similarly, the attenuation coefficient of radiance  $L$  is defined as  $k = -(1/L) dL/dz$ . Attenuation is an apparent optical property (AOP) and depends not only on the properties of the medium, but additionally on the geometric distribution of the illuminating light field.

### 2.3.1 Diffuse attenuation for downwelling irradiance

The most important attenuation coefficient is  $K_d$ , which describes the extinction of downwelling irradiance  $E_d^-$ . The following parameterization is adapted from Gordon (1989), which largely eliminates the light field effect near the surface:

$$K_d(\lambda) = \kappa_0 \cdot \frac{a(\lambda) + b_b(\lambda)}{\cos \theta'_{\text{sun}}} \quad (5)$$

$a(\lambda)$  is calculated according to eq. (3),  $b_b(\lambda)$  using eq. (4).  $\theta'_{\text{sun}}$  is the sun zenith angle in water. The coefficient  $\kappa_0$  depends on the scattering phase function. Gordon (1989) determined a value of  $\kappa_0 = 1.0395$  from Monte simulations in Case 1 waters, Albert and Mobley (2003) found a value of  $\kappa_0 = 1.0546$  from simulations in Case 2 waters using the radiative transfer program Hydrolight (Mobley et al., 1993). Some authors use eq. (5) with  $\kappa_0 = 1$  (Sathyendranath and Platt, 1988, 1997; Gordon et al., 1975). In WASI,  $\kappa_0$  is read from the WASI.INI file; the default value is 1.0546.

### 2.3.2 Diffuse attenuation for upwelling irradiance

For upwelling irradiance two attenuation coefficients are used:  $K_{uW}$  for the radiation backscattered in the water, and  $K_{uB}$  for the radiation reflected from the bottom. The following parameterization is adopted from Albert and Mobley (2003):

$$K_{uW}(\lambda) = [a(\lambda) + b_b(\lambda)] \cdot [1 + \omega_b(\lambda)]^{1.9991} \cdot \left[ 1 + \frac{0.2995}{\cos \theta'_{\text{sun}}} \right] \quad (6)$$

$$K_{uB}(\lambda) = [a(\lambda) + b_b(\lambda)] \cdot [1 + \omega_b(\lambda)]^{1.2441} \cdot \left[ 1 + \frac{0.5182}{\cos \theta'_{\text{sun}}} \right] \quad (7)$$

The function  $\omega_b(\lambda)$  depends on absorption  $a(\lambda)$  and backscattering  $b_b(\lambda)$  of the water body:

$$\omega_b(\lambda) = \frac{b_b(\lambda)}{a(\lambda) + b_b(\lambda)} \quad (8)$$

Eqs. (6) and (7) are used in the model of irradiance reflectance in shallow waters.

### 2.3.3 Attenuation for upwelling radiance

For upwelling radiance two attenuation coefficients are used:  $k_{uW}$  for the radiation backscattered in the water, and  $k_{uB}$  for the radiation reflected from the bottom. The following parameterization is adopted from Albert and Mobley (2003):

$$k_{uW}(\lambda) = \frac{a(\lambda) + b_b(\lambda)}{\cos \theta'_v} \cdot [1 + \omega_b(\lambda)]^{3.5421} \cdot \left[ 1 - \frac{0.2786}{\cos \theta'_{\text{sun}}} \right], \quad (9)$$

$$k_{uB}(\lambda) = \frac{a(\lambda) + b_b(\lambda)}{\cos \theta'_v} \cdot [1 + \omega_b(\lambda)]^{2.2658} \cdot \left[ 1 + \frac{0.0577}{\cos \theta'_{\text{sun}}} \right], \quad (10)$$

where  $\theta'_v$  is the viewing angle in water measured from the nadir direction. These equations are used in the model of remote sensing reflectance in shallow waters.

## 2.4 SPECULAR REFLECTANCE

An above-water radiance sensor looking down to the water surface measures the sum of two radiance components: one from the water body and one from the surface. The first comprises the desired information about the water constituents, the second is an unwanted add-on which requires correction. However, correction is difficult. For example, the method from the SeaWiFS protocols (Mueller and Austin, 1995), which is widely used in optical oceanography, leads to rms errors of the corrected water leaving radiance as large as 90% under typical field conditions (Toole et al., 2000). Thus, WASI offers different methods.

The radiance reflected from the surface,  $L_r(\lambda)$ , is a fraction  $\sigma_L$  of sky radiance  $L_s(\lambda)$ :

$$L_r(\lambda) = \sigma_L \cdot L_s(\lambda). \quad (11)$$

$L_s(\lambda)$  is the average radiance of that area of the sky that is specularly reflected into the sensor. It can be imported from file or calculated using eq. (25).  $\sigma_L$  is the Fresnel reflectance and depends on the angle of reflection. The value can either be specified by the user or it can be calculated from the viewing angle  $\theta_v$  using the Fresnel equation for unpolarized light (Jerlov 1976):

$$\sigma_L = \frac{1}{2} \left| \frac{\sin^2(\theta_v - \theta'_v)}{\sin^2(\theta_v + \theta'_v)} + \frac{\tan^2(\theta_v - \theta'_v)}{\tan^2(\theta_v + \theta'_v)} \right|. \quad (12)$$

$\theta'_v$  is the angle of refraction, which is related to  $\theta_v$  by Snell's law  $n_w \sin \theta'_v = \sin \theta_v$ , where  $n_w \approx 1.33$  is the refractive index of water. For viewing angles near nadir,  $\sigma_L \approx 0.02$ .

The ratio of the radiance reflected from the water surface to the downwelling irradiance,

$$R_{rs}^{\text{surf}}(\lambda) = \frac{L_r(\lambda)}{E_d(\lambda)} = \sigma_L \cdot \frac{L_s(\lambda)}{E_d(\lambda)}, \quad (13a)$$

is called specular reflectance.  $E_d(\lambda)$  and  $L_s(\lambda)$  can either be imported from file, or one or both can be calculated using eq. (23) or (25). If the wavelength-independent model of surface reflection is chosen, it is

$$R_{rs}^{\text{surf}} = \frac{\sigma_L}{\pi}. \quad (13b)$$

Toole et al. (2000) showed that  $R_{rs}^{\text{surf}}(\lambda)$  is nearly spectrally flat for an overcast day, but is not flat for clear-sky conditions. Thus, eq. (13a) should be used in general, and eq. (13b) only for overcast days.

## 2.5 IRRADIANCE REFLECTANCE

### 2.5.1 Deep water

The ratio of upwelling irradiance to downwelling irradiance in water,  $R(\lambda) = E_u(\lambda) / E_d(\lambda)$ , is called irradiance reflectance (Mobley 1994). It is an AOP and depends not only on the properties of the medium, but also on the geometric distribution of the incoming light. A suitable parameterization which separates to a large extent the parameters of water and the illumination conditions was found by Gordon et al. (1975):

$$R(\lambda) = f \cdot \omega_b(\lambda). \quad (14)$$

The function  $\omega_b(\lambda)$ , which is given by eq. (8), depends only on inherent optical properties of the water body, absorption and backscattering. The factor  $f$  comprises the illumination dependencies. It can be treated either as an independent parameter with a default value of 0.33 according to Gordon et al. (1975), or the relationship of Albert and Mobley (2003) can be used:

$$f = 0.1034 \cdot \left(1 + 3.3586 \cdot \omega_b - 6.5358 \cdot \omega_b^2 + 4.6638 \cdot \omega_b^3\right) \cdot \left(1 + \frac{2.4121}{\cos \theta'_{\text{sun}}}\right). \quad (15)$$

$\theta'_{\text{sun}}$  is the sun zenith angle in water. Eq. (15) takes into consideration the fact that  $f$  depends not only on the geometric structure of the light field, expressed by the parameter  $\theta'_{\text{sun}}$ , but also on the absorption and scattering properties of the water, which are included in  $\omega_b$ . The weak dependence of  $f$  on the wind speed is neglected. Some alternate models of  $f$  are also included in WASI and can be used if desired, namely those of Kirk (1984), Morel and Gentili (1991), and Sathyendranath and Platt (1997).

Independently from Gordon, Prieur (1976) found the relation  $R(\lambda) = f' \cdot b_b(\lambda) / a(\lambda)$ . It is also included in WASI. However, the Gordon algorithm (14) is favoured and set as the default, because it restricts the  $\omega_b$  values to the physically reasonable range from 0 to 1, which is not the case for the Prieur equation.

### 2.5.2 Shallow water

For shallow water, the parameterization found by Albert and Mobley (2003) is used:

$$R^{\text{sh}}(\lambda) = R(\lambda) \cdot \left[1 - 1.0546 \cdot \exp\left\{-\left(K_d(\lambda) + K_{uW}(\lambda)\right) \cdot z_B\right\}\right] + 0.9755 \cdot R^b(\lambda) \cdot \exp\left\{-\left(K_d(\lambda) + K_{uB}(\lambda)\right) \cdot z_B\right\} \quad (16)$$

The first term on the right-hand side is the reflectance of a water layer of thickness  $z_B$ , and the second term is the contribution of the bottom. Bottom reflectance  $R^b(\lambda)$  is calculated using eq. (21). The  $K$ 's account for attenuation within the water layer and are calculated using eqs. (5), (6), and (7).

## 2.6 REMOTE SENSING REFLECTANCE

### 2.6.1 Deep water

The ratio of upwelling radiance to downwelling irradiance,  $R_{rs}(\lambda) = L_u(\lambda) / E_d(\lambda)$ , is called remote sensing reflectance (Mobley, 1994). It is an AOP and can be parameterized the same as  $R(\lambda)$  (Albert and Mobley, 2003):

$$R_{rs}^-(\lambda) = f_{rs} \cdot \omega_b(\lambda). \quad (17)$$

Alternately,  $R_{rs}^-$  can be calculated as  $R_{rs}^-(\lambda) = R(\lambda) / Q$ , where  $R(\lambda)$  is either calculated using eq. (14) or imported from file, and  $Q \equiv E_u / L_u$  is treated as a parameter with a default value of 5 sr. A parameterization of the factor  $f_{rs}$ , which can be applied to both deep and shallow waters, was found by Albert and Mobley (2003):

$$f_{rs} = 0.0512 \cdot \left(1 + 4.6659 \cdot \omega_b - 7.8387 \cdot \omega_b^2 + 5.4571 \cdot \omega_b^3\right) \cdot \left(1 + \frac{0.1098}{\cos \theta'_{sun}}\right) \cdot \left(1 + \frac{0.4021}{\cos \theta'_v}\right). \quad (18)$$

Parameters of  $f_{rs}$  are  $\omega_b$  of eq. (8), the sun zenith angle in water,  $\theta'_{sun}$ , and the viewing angle in water,  $\theta'_v$ . Alternately,  $f_{rs}$  can be calculated as  $f_{rs} = f / Q$ .

### 2.6.2 Shallow water

For shallow water, the following parameterization is chosen (Albert and Mobley, 2003):

$$R_{rs}^{sh-}(\lambda) = R_{rs}^-(\lambda) \cdot \left[1 - 1.1576 \cdot \exp\left\{-\left(K_d(\lambda) + k_{uW}(\lambda)\right) \cdot z_B\right\}\right] + 1.0389 \cdot R_{rs}^b(\lambda) \cdot \exp\left\{-\left(K_d(\lambda) + k_{uB}(\lambda)\right) \cdot z_B\right\} \quad (19)$$

The first term on the right-hand side is the reflectance of a water layer of thickness  $z_B$ , the second term the contribution of the bottom. Bottom reflectance  $R_{rs}^b(\lambda)$  is calculated using eq. (22).  $K_d$ ,  $k_{uW}$  and  $k_{uB}$  account for attenuation within the water layer and are calculated using eqs. (5), (9), and (10), respectively.

### 2.6.3 Above the surface

Above the surface, the user can select one of the following parameterizations:

$$R_{rs}(\lambda) = \frac{(1-\sigma)(1-\sigma_L^-)}{n_w^2} \cdot \frac{R_{rs}^-(\lambda)}{1-\sigma^- \cdot Q \cdot R_{rs}^-(\lambda)} + R_{rs}^{surf}(\lambda), \quad (20a)$$

$$R_{rs}(\lambda) = \frac{(1-\sigma)(1-\sigma_L^-)}{n_w^2 \cdot Q} \cdot \frac{R(\lambda)}{1-\sigma^- \cdot R(\lambda)} + R_{rs}^{surf}(\lambda), \quad (20b)$$

$$R_{rs}(\lambda) = \frac{(1-\sigma)(1-\sigma_L^-)}{n_w^2} \cdot \frac{R_{rs}^-(\lambda)}{1-\sigma^- \cdot R(\lambda)} + R_{rs}^{surf}(\lambda). \quad (20c)$$

The three equations are formally identical. A derivation is given in Mobley (1994). The first term on the right-hand side of each equation describes reflection in the water, the second at the surface. Frequently, the first term alone is called remote sensing reflectance (e.g. Mobley 1994). In WASI, the reflection at the surface is also included in the  $R_{rs}$  definition. It is calculated using eq. (13a) or (13b) and can easily be excluded by setting the reflection factor  $\sigma_L$  equal to zero.

$R_{rs}^-(\lambda)$  is calculated using eq. (17) or (19),  $R(\lambda)$  using eq. (14) or (16). The factors  $\sigma$ ,  $\sigma_L^-$ , and  $\sigma^-$  are the reflection factors for  $E_d$ ,  $L_u^-$ , and  $E_u^-$ , respectively.  $\sigma$  depends on the radiance distribution and on surface waves. Typical values are 0.02 to 0.03 for clear sky conditions and solar zenith angles below 45°, and 0.05 to 0.07 for overcast skies (Jerlov 1976; Preisendorfer and Mobley 1985, 1986). The default value is  $\sigma = 0.03$ .  $\sigma_L^-$  can either be calculated as a function of  $\theta_v$  using eq. (12), or a constant value can be inserted.  $\sigma^-$  is in the range of 0.50 to 0.57 with a value of 0.54 considered typical (Jerome et al. 1990; Mobley 1999). The defaults of the other constants are set to  $Q = 5$  sr and  $n_w = 1.33$ .

Selection of the equation to use depends on the application:

- Eq. (20a) links remote sensing reflectance in water to that in air. Since the same spectrum type is used above and below the water surface, it is the most convenient parameterization. This equation is used by default.
- Eq. (20b) is useful when  $R_{rs}(\lambda)$  is linked to  $R(\lambda)$ , for example if *in situ* measurements of  $R(\lambda)$  were performed as “ground truth” for a remote sensing instrument.
- Eq. (20c) avoids the use of the factor  $Q$ , which is difficult to assess. The equation is useful, for example, for optical closure experiments which investigate the consistency of measurements above and below the water surface by measuring simultaneously the spectra  $R_{rs}(\lambda)$ ,  $R(\lambda)$ , and  $R_{rs}^-(\lambda)$ .

## 2.7 BOTTOM REFLECTANCE

The irradiance reflectance of a surface is called albedo. When  $N$  different surfaces of albedo  $a_n(\lambda)$  are viewed simultaneously, the measured albedo is the following sum:

$$R^b(\lambda) = \sum_{n=0}^{N-1} f_n \cdot a_n(\lambda), \quad (21)$$

where  $f_n$  is the areal fraction of surface number  $n$  within the sensor’s field of view; it is  $\sum f_n = 1$ . This equation is implemented in WASI for  $N = 6$  bottom types. Three of the spectra  $a_n(\lambda)$  provided with WASI represent bare bottom, the other green makrophytes: 0 = a constant reflectance of 10 %, 1 = sand, 2 = silt, 3 = *Chara aspera*, 4 = *Potamogeton perfoliatus*, 5 = *Potamogeton pectinatus*. All spectra were measured by Pinnel (2005). The sand spectrum is from a coastal shallow area in South Australia (Bolivar), the other spectra were measured at German lakes (Lake Constance and Starnberger See).

When the upwelling radiation is measured by a radiance sensor, the corresponding remote sensing reflectance can be expressed as follows:

$$R_n^b(\lambda) = \sum_{n=0}^{N-1} f_n \cdot B_n \cdot a_n(\lambda), \quad (22)$$

where  $B_n$  is the proportion of radiation which is reflected towards the sensor. In WASI, the  $B_n$ 's of all surfaces are assumed to be angle-independent. The default values are set to  $B_n = 1/\pi = 0.318 \text{ sr}^{-1}$ , which represents isotropic reflection (Lambertian surfaces).

## 2.8 DOWNWELLING IRRADIANCE

### 2.8.1 Above the water surface

An analytic model of the downwelling irradiance spectrum  $E_d(\lambda)$  using only a few parameters, was developed by Gege (1994, 1995). It fits to measured spectra with a high degree of accuracy (average rms error of 0.1%). The radiation illuminating the water surface is parameterized as the sum of four spectrally different components: (1) the direct solar radiation; (2) the blue sky (Rayleigh) scattering; (3) radiation scattered by aerosols (Mie scattering); and (4) clouds. Each component is expressed in terms of a wavelength-dependent fraction of the extraterrestrial solar irradiance  $E_0(\lambda)$ :

$$E_d(\lambda) = [ \alpha \cdot t_A(\lambda) + \beta \cdot (\lambda/\lambda_R)^{-4.09} + \gamma \cdot (\lambda/\lambda_M)^v + \delta \cdot t_C(\lambda) ] \cdot E_0(\lambda). \quad (23)$$

The four functions  $t_i(\lambda) = \{t_A(\lambda), (\lambda/\lambda_R)^{-4.09}, (\lambda/\lambda_M)^v, t_C(\lambda)\}$  are transmission spectra which spectrally characterize the four light sources. Their weights  $\alpha$ ,  $\beta$ ,  $\gamma$ , and  $\delta$ , may change from one measurement to the next, but the  $t_i(\lambda)$  functions are assumed to be constant over time.

In order to make the weights  $\alpha$ ,  $\beta$ ,  $\gamma$ , and  $\delta$  relative intensities of the four light sources, each is normalized as  $\int t_i(\lambda) E_0(\lambda) d\lambda = \int E_0(\lambda) d\lambda$  where the default integration interval is 400 to 800 nm. The functions  $(\lambda/\lambda_R)^{-4.09}$  and  $(\lambda/\lambda_M)^v$  are calculated during run-time. Normalization yields their scaling factors:  $\lambda_R = 533 \text{ nm}$ , and  $\lambda_M$  is typically between 563 nm ( $v = -1$ ) and 583 nm ( $v = 1$ ). The exponent  $v$  parameterizes the wavelength dependency of aerosol scattering. The remaining functions  $t_A(\lambda)$  and  $t_C(\lambda)$  are read from file. After import they are normalized. The two provided with WASI were determined from measurements at Lake Constance.

### 2.8.2 Below the water surface

The downwelling irradiance in water,  $E_d^-$ , is related to the downwelling irradiance in air,  $E_d$ , through  $E_d^-(\lambda) = (1-\sigma) \cdot E_d(\lambda) + \sigma^- \cdot E_u^-(\lambda)$ .  $\sigma$  is the reflection factor for downwelling irradiance in air,  $\sigma^-$  for upwelling irradiance in water, and  $E_u^-$  is the upwelling irradiance in water. Using the irradiance reflectance  $R = E_u^- / E_d^-$  yields the following expression:

$$E_d^-(\lambda) = \frac{1-\sigma}{1-\sigma^- \cdot R(\lambda)} \cdot E_d(\lambda). \quad (24)$$

This equation is used in WASI for calculating  $E_d^-(\lambda)$ .  $R(\lambda)$  is calculated using eq. (14).  $E_d(\lambda)$  can either be calculated according to eq. (23) or a measured spectrum can be taken. Default values of the reflection factors are  $\sigma = 0.03$  and  $\sigma^- = 0.54$ .

## 2.9 SKY RADIANCE

The parameterization used for  $E_d(\lambda)$  is also implemented for  $L_s(\lambda)$ :

$$L_s(\lambda) = [ \alpha^* \cdot t_A(\lambda) + \beta^* \cdot (\lambda/\lambda_R)^{-4.09} + \gamma^* \cdot (\lambda/\lambda_M)^v + \delta^* \cdot t_C(\lambda) ] \cdot E_0(\lambda). \quad (25)$$

The functions  $E_0(\lambda)$ ,  $t_A(\lambda)$ ,  $(\lambda/\lambda_R)^{-4.09}$ ,  $(\lambda/\lambda_M)^v$ , and  $t_C(\lambda)$  are those used with eq. (23). Parameters of  $L_s(\lambda)$  are the weights  $\alpha^*$ ,  $\beta^*$ ,  $\gamma^*$ , and  $\delta^*$ , which represent the relative intensities of the four above-mentioned light sources for a radiance sensor, and the exponent  $v$ .

This model of  $L_s(\lambda)$  is included for modeling specular reflection at the water surface. Its usefulness has been demonstrated (Gege, 1998b). Capillary waves at the water surface, and moreover gravity waves, increase the sky area that is reflected into the sensor, and change the angle of reflection. Consequently, measurements of  $L_s(\lambda)$  are frequently not reliable. For these cases, and if no  $L_s(\lambda)$  measurement is available, eq. (25) can be applied. If the user selects the wavelength-independent model of surface reflections,  $L_s(\lambda) = E_d(\lambda)/\pi$  is utilized.

## 2.10 UPWELLING RADIANCE

The upwelling radiance is that part of the downwelling irradiance which is reflected back from the water into a down-looking radiance sensor. Calculation is based on a model of  $R_{rs}$  and a model or a measurement of  $E_d$ .

In water, eq. (24) is used for calculating  $E_d^-(\lambda)$ , and eq. (17) or (19) for  $R_{rs}^-(\lambda)$ . The upwelling radiance is then calculated as follows:

$$L_u^-(\lambda) = R_{rs}^-(\lambda) \cdot E_d^-(\lambda). \quad (26)$$

In air, the upwelling radiance after crossing the water-air boundary is related to  $L_u^-$  as follows:

$$L_u(\lambda) = \frac{1 - \sigma_L^-}{n_w^2} \cdot L_u^-(\lambda) + L_r(\lambda). \quad (27)$$

The first term on the right-hand side is the radiance upwelling in the water, weakened at the interface by Fresnel reflection (factor  $1 - \sigma_L^-$ ) and refraction (flux dilution by widening of the solid angle, factor  $1/n_w^2$ ).  $L_u^-(\lambda)$  is obtained from eq. (26),  $L_r(\lambda)$  from eq. (11).  $\sigma_L^-$  can either be calculated as a function of  $\theta_v$  using eq. (12), or a constant value can be used. Default values of the constants are  $\sigma_L^- = 0.02$  and  $n_w = 1.33$ .

## 3. Inverse Modeling

Inverse modeling is the determination of model parameters for a given spectrum. The complete list of model parameters for all spectrum types is given in Table 2. These can be iterated in the forward mode to generate series of spectra, and their values can be determined in the inverse mode. The user defines which parameters are determined during inversion and which are kept constant. The former are called *fit parameters*. The actual number of fit parameters depends on the spectrum type, on model options, and on the user's choice of which parameters to fit and which to fix during inversion.

**Table 2.** List of WASI parameters.

Symbol	WASI	Units	Description
$C_i$	C[i]	$\mu\text{g/l}$	Concentration of phytoplankton class no. $i$ , $i = 0..5$
$C_L$	C_L	$\text{mg/l}$	Concentration of large suspended particles
$C_S$	C_S	$\text{mg/l}$	Concentration of small suspended particles
$X$	C_X	$\text{m}^{-1}$	Concentration of non-chlorophyllous particles
$Y$	C_Y	$\text{m}^{-1}$	Concentration of Gelbstoff
$S$	S	$\text{nm}^{-1}$	Exponent of Gelbstoff absorption
$n$	n	-	Exponent of backscattering by small particles
$T$	T_W	$^{\circ}\text{C}$	Water temperature
$f$	f	-	Proportionality factor of reflectance ("f-factor")
$Q$	Q	sr	Anisotropy factor ("Q-factor")
$\theta_{\text{sun}}$	sun	$^{\circ}$	Sun zenith angle
$\theta_v$	view	$^{\circ}$	Viewing angle ( $0 = \text{nadir}$ )
$\sigma_L$	sigma_L	-	Reflection factor of sky radiance
$z_B$	zB	m	Bottom depth
$\nu$	nue	-	Exponent of aerosol scattering
$\alpha$	alpha	-	Fraction of irradiance due to direct solar radiation
$\beta$	beta	-	Fraction of irradiance due to molecule scattering
$\gamma$	gamma	-	Fraction of irradiance due to aerosol scattering
$\delta$	delta	-	Fraction of irradiance due to cloud scattering
$\alpha^*$	alpha_s	$\text{sr}^{-1}$	Fraction of radiance due to direct solar radiation
$\beta^*$	beta_s	$\text{sr}^{-1}$	Fraction of radiance due to molecule scattering
$\gamma^*$	gamma_s	$\text{sr}^{-1}$	Fraction of radiance due to aerosol scattering
$\delta^*$	delta_s	$\text{sr}^{-1}$	Fraction of radiance due to cloud scattering
$f_n$	fA[n]	-	Areal fraction of bottom surface type no. $n$ , $n = 0..5$

### 3.1 IMPLEMENTED METHOD

#### 3.1.1 Curve fitting

The fit parameters are determined iteratively using the method of nonlinear curve fitting. In the first iteration, a model spectrum is calculated using initial values for the fit parameters. This model spectrum is compared with the measured spectrum by calculating the residuum as a measure of correspondence. Then, in the further iterations, the values of the fit parameters are altered, resulting in altered model curves and altered residuals. The procedure is stopped after the best fit between the calculated and measured spectrum is found. The best fit corresponds to the minimum residuum, and these values are the estimates of fit parameters.

#### 3.1.2 Search algorithm

Since an infinite number of possible parameter combinations exists, an effective algorithm of the iteration process is needed to select a new set of parameter values from the previous sets. WASI uses the Simplex algorithm (Nelder and Mead, 1965; Caceci and Cacheris, 1984). It has two advantages compared to other customary algorithms like Newton-Ralphson and Levenberg-Marquardt: it always converges, and computations are rapid since no matrix operations are required.

In the Simplex algorithm, a virtual space of  $M+1$  dimensions is constructed, where  $M$  dimensions represent the  $M$  fit parameters, and one dimension the residuum. Each model curve corresponds to one point in that space, and the set of all possible model

curves (obtained by all combinations of parameter values) forms an  $M$  dimensional surface. That point on the surface where the residuum is minimal represents the solution of the fit problem. The Simplex can be compared to a spider which crawls on the surface searching for the minimum. It consists of  $M+1$  legs, where each leg (vertex) represents a model curve that has already been calculated. The decision regarding which set of parameter values is chosen in the next step (i.e. where the Simplex moves to) is made according to a strategy explained using Figure 2.

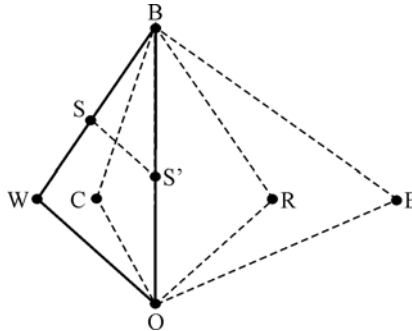


**Figure 2.** The Simplex and its potential contours in the next step. After Caceci and Cacheris (1984).

The triangle WBO represents the Simplex. W corresponds to the worst residuum, B to the best, and O to all others. Four new positions in the next step are considered: (1) reflection of W at the line OB so that RBO is the new Simplex; (2) contraction towards this line so that CBO is the new Simplex; (3) expansion beyond this line to the point E; (4) shrinkage parallel to the line WO so that SBS' is the new Simplex. Not all of these positions are always calculated: they are tested in this order, and the first position is taken where the new vertex is better than W. Usually the Simplex is trapped in a minimum after less than  $20 \cdot M^2$  iterations (Caceci and Cacheris, 1984). However, if the surface contains local minima, the Simplex may be captured in one of these. In such cases it is important to start the search at a point not too far away from the global minimum.

### 3.1.3 Modes of operation

Three modes of operation are implemented in WASI:

- *Single spectrum mode.* Fitting is performed for a single spectrum. After inversion, an overlay of the spectrum and fitted curve is automatically shown on screen and the resulting fit values, number of iterations, and residuum are displayed. This mode allows the user to inspect the fit results of individual measurements. This mode is useful for optimizing the choice of initial values and the fit strategy before starting a batch job.
- *Batch mode.* A series of spectra from file is fitted. After each inversion, an overlay of the imported spectrum and fitted curve is automatically shown on screen. This mode is useful for processing large data sets.

- *Reconstruction mode.* Combines forward and inverse modes. Inversion is performed for a series of forward calculated spectra which are not necessarily read from file. The model parameters can be chosen differently for forward and inverse calculations. This mode is useful for performing sensitivity studies.

### 3.2 INVERSION PROBLEMS

#### 3.2.1 Ambiguity

When different sets of model parameters yield similar spectra, the inversion problem is ambiguous. In such a case, no algorithm can reliably find the correct values of the fit parameters. The problem is model specific and increases drastically with the number of fit parameters.

An example is given in Figure 3. Three absorption spectra  $a_{WC}(\lambda)$  were calculated using eq. (1) by summing the absorptions of phytoplankton chlorophyll (concentration  $C_0$ ) and Gelbstoff (concentration  $Y$ , spectral slope  $S$ ). The concentrations  $C_1, \dots, C_5$  and  $X$  were set to zero. The curves are almost identical from 400 to 600 nm, but have very different parameter values: the parameter set  $(C_0, Y, S)$  is  $(2, 0.2, 0.014)$  for curve A,  $(1, 0.232, 0.0124)$  for curve B, and  $(4, 0.132, 0.020)$  for curve C. Thus, although phytoplankton concentration differs by a factor of 4, the three curves can hardly be distinguished between 400 to 600 nm. It is consequently not possible to determine all three parameters  $C_0, Y, S$  from measurements in this spectral range, since any inversion method compensates for error with one parameter by using erroneous values for the two other parameters. There are two solutions to this type of problem: 1) at least one of the parameters must be known and kept constant during inversion, 2) the spectral range must be extended to wavelengths above 600 nm.

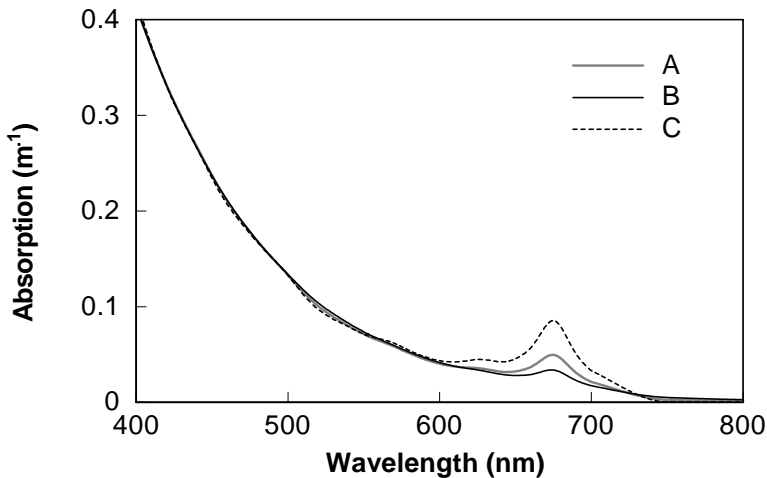


**Figure 3.** Illustration of the ambiguity problem. Although phytoplankton concentration  $C_0$  differs by a factor of 4, the three spectra are very similar from 400 to 600 nm. The changes caused by  $C_0$  are compensated by changes of the Gelbstoff parameters  $Y$  and  $S$ .

### 3.2.2 Failure to converge

An inversion algorithm doesn't always find a minimum. Several conditions can cause such a failure to converge:

- *Initial increments are too small.* If the initial steps of the search algorithm are too small, the differences in the residuals are too small to indicate an improvement for a particular parameter combination compared to others. Depending on the criterion for termination, this may cause premature conclusion, or travelling in the wrong direction in the multidimensional parameter space.
- *Acceptable errors are too large.* If the criterion for terminating inversion is chosen as too weak, the inversion algorithm may stop too early, before the minimum is found.
- *Unsuited initial values.* If the initial values of the fit parameters are too different from the correct values, the search for the minimum may start in a wrong direction. The greater the number of fit parameters, the more difficult it is to find the correct region in the multidimensional parameter space.

## 3.3 PROBLEM SOLUTIONS OF WASI

### 3.3.1 Use of pre-knowledge

In WASI, one can make use of expected parameter values. Typical values of all parameters and constants are stored in the file WASI.INI, which is read during start up of the program. The user can change them all. The parameters which are fitted during inversion can be initialised either with these expected values, or with estimates calculated by using analytic approximations (see 3.3.3). When a series of spectra is analyzed, the parameter values may be similar. Thus, the fit results of one measurement can be taken as start values for the next.

The parameter range can also be modified. The range of possible values is known in general for each parameter, and within WASI a lower and an upper value is attributed to each fit parameter. The defaults of these border values are read during program start from the WASI.INI file, and the user can change them. They are used whenever the search algorithm attempts to assign an out-of-range value to a parameter.

When a well-known correlation exists between model parameters, it may be useful to restrict a parameter search to values which depend on the actual values of one or more other parameters. No general scheme of this method (regularization) is implemented in WASI. However, some correlations between parameters can be utilized. For example, suspended matter can be correlated to phytoplankton chlorophyll by setting  $C_L = C_0$  (see 2.2.1); the reflection factor for sky radiance can be related to the viewing angle using the Fresnel equation (12); and the areal fraction  $f_n$  of one bottom type can be related to the fractions of the other types using  $\sum f_n = 1$  (see 2.7).

### 3.3.2 Adjust calculation of the residuum

The residuum,  $\Delta$ , is the measure of the difference between a measured spectrum and its fitted curve. The inversion procedure's task is to find its minimum. The residuum can be envisaged as a surface in the  $M+1$  dimensional space formed by the  $M$  fit parameters and by  $\Delta$ . The shape of that surface depends on which construction law is

used. Thus, the search for the minimum can be optimized by adjusting the construction law to the inversion problem.

*Algorithms.* The user has the choice between 6 algorithms to calculate  $\Delta$ :

$$\Delta = \frac{1}{N} \sum_{i=1}^N g_i \cdot |m_i - f_i|^2 \quad (28a)$$

$$\Delta = \frac{1}{N} \sum_{i=1}^N g_i \cdot |m_i - f_i| \quad (28b)$$

$$\Delta = \frac{1}{N} \sum_{i=1}^N g_i \cdot \left| 1 - \frac{f_i}{m_i} \right|^2 \quad (28c)$$

$$\Delta = \frac{1}{N} \sum_{i=1}^N g_i \cdot |\ln(m_i) - \ln(f_i)|^2 \quad (28d)$$

$$\Delta = \frac{1}{N} \sum_{i=1}^N g_i \cdot |\ln(m_i) - \ln(f_i)| \quad (28e)$$

$$\Delta = \frac{1}{N} \sum_{i=1}^N g_i \cdot \left| 1 - \frac{\ln(f_i)}{\ln(m_i)} \right|^2 \quad (28f)$$

The residuum is a weighted sum over  $N$  spectral channels. The subscript  $i$  indicates the channel number,  $m_i$  denotes the measured value,  $f_i$  the fit value, and  $g_i$  the weight. Eq. (28a) in combination with  $g_i = 1$  is the classical least-squares fit. During inversion the  $f_i$  values are changed, but not the  $m_i$  and  $g_i$  values.

The impact of residuum algorithm selection on the shape of the surface in the parameter space is illustrated in the example of Figure 4. Two contour plots of the residuum are shown for an inversion of absorption spectra, which were calculated using eq. (1) by summing the absorptions of phytoplankton and Gelbstoff. In this example the concentrations  $C_1, \dots, C_5$  and  $X$  were set to zero. Phytoplankton chlorophyll concentration  $C_0$  was set to  $2 \mu\text{g/l}$  during forward and inverse calculation. The Gelbstoff parameters were set to  $S = 0.014 \text{ nm}^{-1}$  and  $Y = 0.3 \text{ m}^{-1}$  during forward calculation and then were iterated from  $0.01 \text{ nm}^{-1} \leq S \leq 0.02 \text{ nm}^{-1}$  and  $0 \leq Y \leq 0.6 \text{ m}^{-1}$  during inversion. No fit was performed during inversion; only the residuum was calculated for each parameter combination with equal weights  $g_i = 1$ .

The major difference between the two plots of Fig. 4 is the orientation of the valley which forms the minimum: the valley is almost parallel to the  $S$  axis for the classical least-squares fit (eq. 28a), i.e. the inversion cannot determine  $S$  reliably. When the logarithms of the  $m_i$  and  $f_i$  are taken (eq. 28d), the valley is oriented diagonally in the  $S$ - $Y$ -plane, and thus fitting of both  $S$  and  $Y$  is feasible. For the concentrations chosen, eq. (28d) is more appropriate because the absorption spectrum is dominated by the exponential function of Gelbstoff.

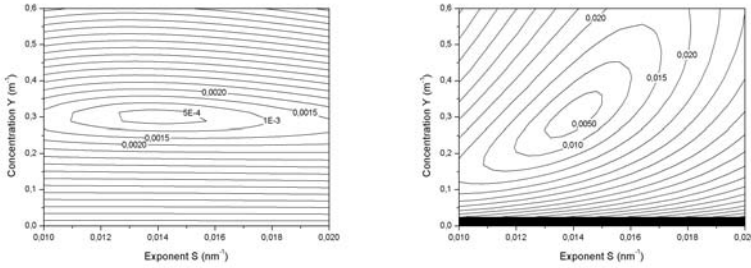


**Figure 4.** Contour plots of the residuum at inversion of absorption spectra. Both plots correspond to a least-squares fit. Left: Linear weighting of absorption values (eq. 28a). Right: Logarithmic weighting of absorption values (eq. 28d).

*Spectral range and data interval.* The user can select the channels  $i$  which will be taken for residuum calculation by specifying the upper and lower boundaries and channel interval. Modern instruments frequently provide hundreds of spectral channels. It is usually not necessary to use each channel for inversion. Reducing the number of channels reduces calculation time.

*Spectral weighting.* The channels are weighted individually such that their weights  $g_i$  are read from file. The default file is EINS.PRN, which sets all  $g_i$  to unity. The selection of different  $g_i$ 's allows the user to exclude certain spectral regions or to weight the information spectrally. This feature is useful if the measurement or the model is not reliable in certain spectral intervals. For example, since the models do not include chlorophyll fluorescence at 685 nm, it may be useful to exclude channels around 685 nm or give them low weights.

### 3.3.3 Automatic determination of initial values

Making a good guess for the fit parameters' initial values is the best way to reduce all types of inversion problems. Thus, for operational data analysis it is desirable to have an automatic algorithm which estimates initial values for the most relevant parameters with acceptable errors. Such automatic methods are implemented for  $R$  and  $R_{rs}$  spectra. The case for  $R$  in deep water is described below, while those for  $R$  and  $R_{rs}$  in shallow waters are explained in Albert (2004) and Albert and Gege (2005).

*Example:  $R$  in deep water.* Irradiance reflectance  $R(\lambda)$  is one of the most frequently measured spectrum types in optically deep waters. The most common parameters determined from these measurements are the concentrations of phytoplankton ( $C_0$ ), Gelbstoff ( $Y$ ) and large suspended particles ( $C_L$ ). Gege (2002b) investigated the sensitivity of these fit parameters to errors. The study demonstrated a very small sensitivity for  $C_L$ , some sensitivity for  $Y$ , but very high sensitivity for  $C_0$ . Considering error propagation, the study suggested a two-steps procedure for initial values determination. The procedure has been further optimised, resulting in the four-step procedure summarized in Table 3 and presented below.

**Table 3.** Four-step procedure for initial values determination of irradiance reflectance spectra in deep water.

Step	Determine	Algorithm	Description
1	$C_L, C_S$	analytical	Estimate $C_L$ and $C_S$ from an analytic equation at a wavelength in the near infrared.
2	$Y, C_0$	analytical	Estimate $Y$ and $C_0$ from analytic equations at two wavelengths; for $C_L$ and $C_S$ the values from step 1 are taken.
3	$C_L, C_S, Y$	fit	Determine initial values of $C_L, C_S$ and $Y$ by fit. $C_0$ is kept constant at the value from step 2; $C_L, C_S$ and $Y$ are initialized using the values from steps 1 and 2.
4	$C_0, Y, S$	fit	Determine initial values of $C_0, Y$ and $S$ by fit. $C_L$ is kept constant at the value from step 3, $Y$ is initialized using the value from step 3, $S$ is initialized by the user-setting.

**Step 1.** Suspended matter backscattering,  $B_0 = b_b - b_{b,W}$ , can be calculated analytically from  $R$  at any wavelength  $\lambda_{IR}$  for which absorption  $a(\lambda_{IR})$  is known. For  $\lambda_{IR}$  a wavelength in the near infrared is chosen since absorption of water constituents is generally very low compared to absorption of pure water at  $\lambda > 700$  nm (Babin and Stramski, 2002). Ideally,  $\lambda_{IR} > 750$  nm should be used, since phytoplankton absorption  $a_0^*(\lambda)$  is zero above 750 nm. The equation of determination is obtained from eqs. (8) and (14):

$$B_0 = \frac{a(\lambda_{IR}) \cdot R(\lambda_{IR})}{f - R(\lambda_{IR})} - b_{b,W}(\lambda_{IR}). \quad (29)$$

$f$  is calculated using the selected  $f$  model, e.g. eq. (15), with the user-defined initial values as parameter values. If a  $B_0$ -dependent  $f$  model is selected,  $B_0$  is calculated in two iterations, i.e. the  $B_0$  value from the first iteration is taken to calculate  $f$  again, and using this  $f$   $B_0$  is calculated a final time.

Conversion from optical units  $B_0$  to gravimetric concentrations  $C_L, C_S$  is based on eq. (4) assuming  $b_L(\lambda) = 1$ . Accordingly it is  $B_0 = C_L \cdot b_{b,L}^* + C_S \cdot b_{b,S}^* \cdot (\lambda/\lambda_S)^n$ . If  $C_S = 0$ , it is  $C_L = B_0 / b_{b,L}^*$ , otherwise the user-defined ratio  $r_{SL} = C_S/C_L$  is retained, and  $C_L$  and  $C_S$  are calculated as follows:

$$C_L = \frac{B_0}{b_{b,L}^* + r_{SL} \cdot b_{b,S}^* \cdot \left(\frac{\lambda_{IR}}{\lambda_S}\right)^n}; \quad C_S = r_{SL} \cdot C_L. \quad (30)$$

If  $\lambda_{IR} > 750$  nm, the accuracy of the analytically estimated parameters  $C_L$  and  $C_S$  depends only on  $\lambda_{IR}$ , Gelbstoff absorption at  $\lambda_{IR}$ , and on  $C_L$  and  $C_S$  themselves. The dependence of the relative  $C_L$  error on  $Y$  and  $C_L$  is shown in Fig. 5 for two values of  $\lambda_{IR}$ , 750 and 870 nm. It was calculated as  $100 \cdot (C_L/C_L^{fwd} - 1)$ , where  $C_L^{fwd}$  is the value of forward calculation and  $C_L$  the value obtained from eq. (30). Values of  $S = 0.014 \text{ nm}^{-1}$  and  $C_S = 0$  were used. As Figure 5 shows,  $C_L$  can be determined using eqs. (29) and (30) with an accuracy of about 1%.

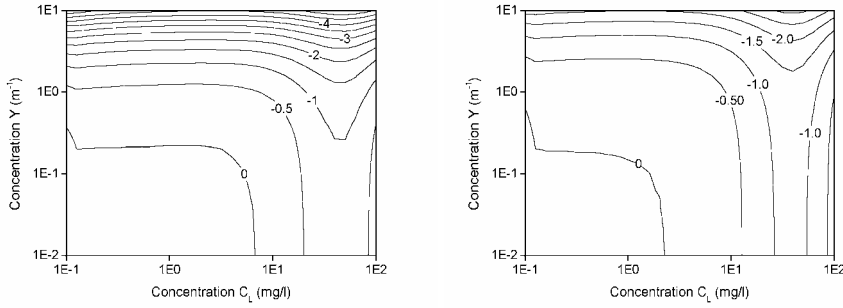


**Figure 5.** Relative errors in percent for analytic determination of  $C_L$ . Left:  $\lambda_{IR} = 750$  nm, Right:  $\lambda_{IR} = 870$  nm.

**Step 2.** If  $b_b(\lambda)$  is known with little error, e.g. from step 1,  $C_0$  and  $Y$  can be estimated analytically from two wavelengths  $\lambda_1, \lambda_2$ . The equations of determination are obtained by using the  $R(\lambda)$  equation (14) and setting  $C_1 \dots C_5 = 0, T = T_0, X = 0$ . This eq. (14') is solved for the sum  $Y \cdot a_Y^*(\lambda) + C_0 \cdot a_0^*(\lambda)$ , and the ratio  $R_A$  is taken for two wavelengths:

$$R_A := \frac{Y \cdot a_Y^*(\lambda_1) + C_0 \cdot a_0^*(\lambda_1)}{Y \cdot a_Y^*(\lambda_2) + C_0 \cdot a_0^*(\lambda_2)} = \frac{f \cdot \frac{b_b(\lambda_1)}{R(\lambda_1)} - a_w(\lambda_1) - b_b(\lambda_1)}{f \cdot \frac{b_b(\lambda_2)}{R(\lambda_2)} - a_w(\lambda_2) - b_b(\lambda_2)}. \quad (31)$$

Since all functions on the right-hand side are known,  $R_A$  can be calculated. Division of the nominator and denominator of the center expression by  $C_0$  leads to an equation which has a single unknown parameter, the ratio  $Y/C_0$ . Rewriting this equation yields the following expression:

$$\frac{Y}{C_0} = \frac{R_A \cdot a_0^*(\lambda_2) - a_0^*(\lambda_1)}{a_Y^*(\lambda_1) - R_A \cdot a_Y^*(\lambda_2)}. \quad (32)$$

The ratio  $Y/C_0$  is calculated using this equation. By inserting  $Y = (Y/C_0) \cdot C_0$  into eq. (14') and solving it for  $C_0$  at a wavelength  $\lambda_3$ , the following expression is obtained:

$$C_0 = \frac{f \cdot \frac{b_b(\lambda_3)}{R(\lambda_3)} - a_w(\lambda_3) - b_b(\lambda_3)}{a_0^*(\lambda_3) + \frac{Y}{C_0} \cdot a_Y^*(\lambda_3)}. \quad (33)$$

This equation is used to calculate  $C_0$ .  $Y$  is then calculated as  $Y = (Y/C_0) \cdot C_0$ .

The accuracy of the analytically estimated parameters  $C_0$  and  $Y$  depends on  $\lambda_1, \lambda_2, \lambda_3, C_0, Y, C_L, C_S$ , and on the errors of  $C_L$  and  $C_S$ , as determined from step 1. Simulations were performed to optimize the choice of the wavelengths  $\lambda_1, \lambda_2, \lambda_3$ . These suggest:  $\lambda_1 < 470$  nm,  $\lambda_2 < 500$  nm,  $\lambda_3 < 550$  nm. In each case, preference should be

given to shorter wavelengths. A good choice is  $\lambda_2 = \lambda_0$  since S errors don't affect Gelbstoff absorption at  $\lambda_0$ . For  $\lambda_3$  no separate wavelength must be chosen, and it can be set as  $\lambda_3 = \lambda_2$ . Consequently, selection of only two wavelengths is implemented in WASI. Their default values are:  $\lambda_1 = 413$  nm,  $\lambda_2 = 440$  nm.

In order to illustrate the parameter dependencies and magnitudes of the  $C_0$  and Y errors, Figure 6 presents two examples of these errors.  $R(\lambda)$  spectra were calculated using eq. (14) with  $\omega_b(\lambda)$  from eq. (8) and  $f$  from eq. (15). All non-iterated parameters were set equal during forward and inverse calculation:  $C_0 = 2$   $\mu\text{g/l}$ ,  $C_1 \dots C_5 = 0$ ,  $X = 0$ ,  $Y = 0.2$   $\text{m}^{-1}$ ,  $C_S = 0$ ,  $S = 0.014$   $\text{nm}^{-1}$ ,  $\theta_{\text{sun}} = 30^\circ$ ,  $T = 18^\circ\text{C}$ .  $C_L$  was iterated from 0.1 to 100  $\text{mg/l}$ , and for Figure 6A Y was iterated from 0.01 to 10  $\text{m}^{-1}$ , for Figure 6B  $C_0$  was iterated from 0.1 to 100  $\mu\text{g/l}$ . All iterations were done in 51 steps such that the logarithmic values were equidistant. Thus, both plots in Figure 6 consist of  $51 \cdot 51 = 2601$  data points, where each point represents the absolute error  $100 \cdot |c/c^{\text{fw}} - 1|$  of the concentration  $c$ , Y for Figure 6A and  $C_0$  for Figure 6B.  $c^{\text{fw}}$  is the concentration at forward calculation, and  $c$  is the retrieved value. Figure 6 indicates that Y can be determined analytically with a typical accuracy of  $< 30$  %, and  $C_0$  of about 30–100 %. This is sufficient for initial values.

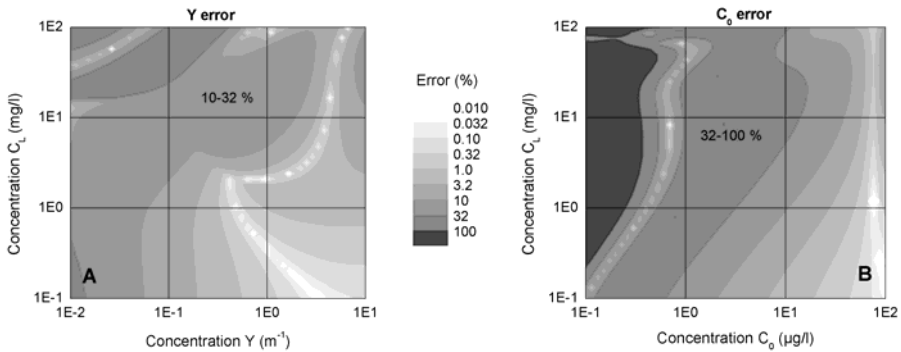


**Figure 6.** Relative errors of analytic determination of (A) Y error and (B)  $C_0$  error.

**Steps 3 and 4.** These steps were suggested in the study mentioned above (Gege, 2002b). Newly developed Steps 1 and 2 make them unnecessary in most cases. However, they may be useful under certain conditions: if no suitable infrared channel is available for accurate determination of  $C_L$  or  $C_S$ , or if S is a fit parameter. Steps 3 and 4 improve the estimates for  $C_0$ ,  $C_L$ ,  $C_S$  and Y by including additional spectral information, and a start value of S can be determined.

### 3.3.4 Initialize Simplex

The search algorithm's dynamic memory, the Simplex, is a set of  $M+1$  vectors. Each vector (or vertex) contains the actual values of the  $M$  fit parameters and the corresponding residuum. When the fit routine is started, the  $M+1$  vertices are initialized. The fit parameters' initial values and the corresponding residuum form one vertex and the other  $M$  vertices are calculated using incremental changes of the initial values. These increments are set to 0.1 x the initial values. They cannot be changed by the user.

### 3.3.5 Terminate search

The fit is stopped when either the termination criterion is fulfilled or the maximum number of iterations is reached. The termination criterion is such that the differences between the actual parameter values must be less than a threshold for each parameter. Each parameter has its specific threshold, which is set to  $10^{-5}$  times the initial value. It cannot be changed by the user. The user defines the maximum number of iterations, which should be set high enough that a forced stop is exceptional.

## 4. Applications

### 4.1 DATA ANALYSIS

Automatic data analysis of a series of spectra is performed in the batch mode within WASI. The spectra must be in ASCII format. The following user actions are required:

1. Copy all spectra into the same directory
2. Specify the directories of input and output data
3. Specify file names and file format of the input data
4. Set the batch mode
5. Specify the spectrum type
6. Tune the fit procedure
7. Set the model parameters
8. Select the fit parameters
9. Start calculation

The results are stored in ASCII format in the specified output directory. A single table, FITPARS.TXT, summarizes the fit parameters of all spectra. All calculation settings are documented in an actual copy of the file WASI.INI. The fit curves of all spectra can be saved as single files.

### 4.2 ERROR ANALYSIS

No measurement is perfect, no model is exact, and no input data set is complete. Thus, the results of data analysis are unavoidably affected by errors. Sensitivity studies are designed to estimate the errors for a determined parameter caused by the different error sources. The best way to perform a sensitivity study is to simulate a large number of measurements using a reliable model, and to then analyze these subsequently as if they were real measurements. Well-defined discrepancies between the forward and inverse models can be introduced which cause errors in the retrieved parameters. In this way, parameter errors can be attributed quantitatively to different error sources. The advantages of using simulated spectra rather than measured spectra are that all studied effects are under control, and that the entire expected parameter interval can be covered without a gap.

#### 4.2.1 Errors from the sensor

The number of parameters that can be derived from a measurement and the accuracy of the estimates depends very much on the sensor and on data quality. The following instrument characteristics are relevant: number, center wavelengths and

spectral resolutions of spectral channels; radiometric resolution; accuracy of radio-metric and spectral calibration; noise; and drift.

For estimating the limits of accuracy caused by the sensor, spectra of the given sensor are simulated for different combinations of model parameters, and spectra of a “perfect” sensor are calculated for the same combinations. Both sets of spectra are inverted, and the accuracies of the fit parameters are compared.

Sensor characteristics which are readily defined and changed easily using WASI are number and center wavelengths of the channels, radiometric resolution, and statistical noise. For studying the influence of spectral resolution and calibration accuracy, WASI can be used to calculate spectra which are sensor-adjusted with respect to the number and center wavelengths of the channels, radiometric resolution, and statistical noise. These spectra are then modified according to the instrument characteristics: the spectra are smoothed if the instrument has a lower spectral resolution than the input data, error spectra are added and/or multiplied to the spectra if radiometric calibration errors are investigated, and the wavelength values are changed if spectral calibration errors are analyzed. This is done using separate software, such as a spread sheet program. Finally, the sensor-adjusted spectra are inverted using WASI.

An example is given in Figure 7. Absorption spectra of water constituents were simulated for 4 sensors which differ in the number of spectral channels and in the noise level: spectra  $a_{WC}(\lambda)$  were calculated using eq. (1) from 400 to 800 nm for wavelength intervals of 2 and 20 nm and statistical noise of 0.002 and 0.02  $m^{-1}$  standard deviation. The Gelbstoff parameters chosen were  $Y = 0.2 m^{-1}$  and  $S = 0.014 nm^{-1}$ . Concentrations  $C_1, \dots, C_5$  and  $X$  were set to zero. Phytoplankton chlorophyll concentration  $C_0$  was changed from 0.1 to 100  $\mu g/l$  in 51 steps. 20 spectra  $a_{WC}(\lambda)$  were calculated for each  $C_0$  value by applying a simple trick: a parameter not used in the actual model was iterated during forward calculation. Each of the  $51 \cdot 20 = 1020$  spectra for each sensor was inverted with  $C_0$  and  $Y$  as fit parameters. Figure 7 compares the  $C_0$ -dependency of the relative  $C_0$  errors for the 4 sensor specifications.  $C_0$  errors are more sensitive to noise than to the number of channels in this example.

#### 4.2.2 Errors from the model

The radiative transfer equation for an absorbing and scattering medium like water cannot be solved analytically, hence observations which depend on the radiation field (AOPs) can only be approximated. WASI uses analytic approximations based on parameters which can be measured with relative ease. Advantages are that inversion is relatively simple, altered input data sets are included quickly, and computing is fast.

From a numerical point of view, any desired accuracy can be achieved by using converging methods such as Monte Carlo, invariant imbedding, matrix operator, successive order of scattering, finite elements, etc. However, high accuracy is at the expense of computing time, which, for these methods, is by far too long for inverting a set of spectra. In order to estimate errors introduced by the approximations of WASI, a set of spectra must be calculated using a numerically exact program, and for the same conditions a second set of spectra is calculated using WASI. Both sets of spectra are inverted, and the differences of the fit parameters reflect the errors introduced by the simplified model.

An example is given in Figure 8. Remote sensing reflectance spectra of shallow water were calculated using both HYDROLIGHT (Mobley et al., 1993, Mobley, 1994) and WASI (eq. 19). All input data and parameters for the two models were identical.

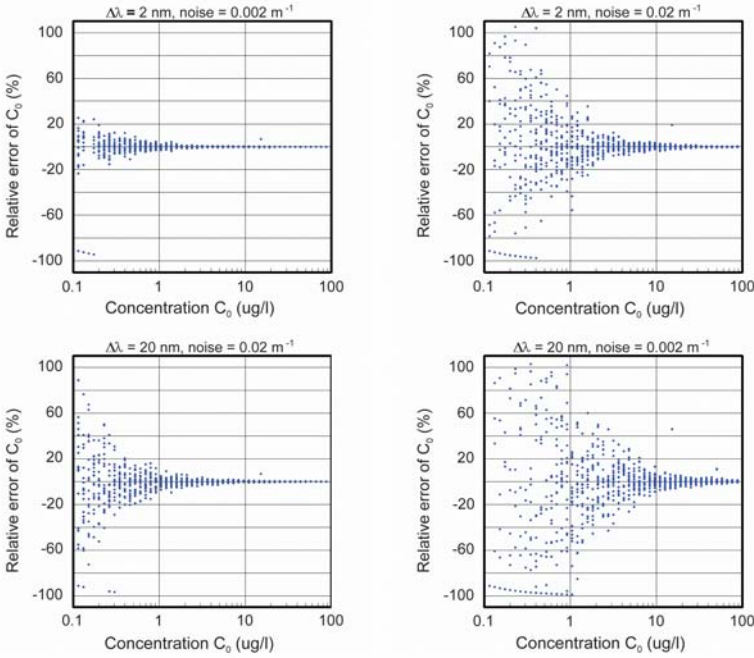


**Figure 7.** Illustration of errors from a sensor for an example of absorption measurements. The plots show errors for inverse modelling of phytoplankton concentration resulting from adjusting spectral width of channels and sensor noise.

Water constituent values were:  $C_0 = 2 \mu\text{g/l}$ ;  $Y = 0.3 \text{ m}^{-1}$ ;  $S = 0.014 \text{ nm}^{-1}$ .  $C_L$  was iterated from 1 to 5 mg/l. The lake sediment spectrum provided with WASI was used for the bottom albedo. Computing times of HYDROLIGHT, which utilizes the invariant imbedding method, were typically  $10^6$  times longer than those for WASI.

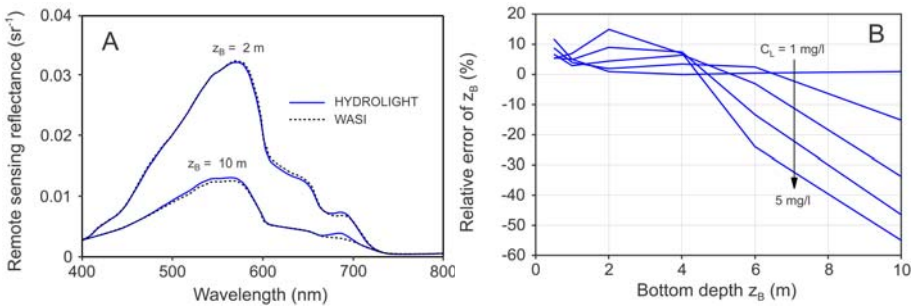


**Figure 8.** Illustration of errors from the model using an example of remote sensing reflectance spectra. A: Comparison of spectra from the numerically extensive program HYDROLIGHT with WASI. B: Errors of bottom depth when WASI is used for inverting HYDROLIGHT spectra.

Figure 8A compares the HYDROLIGHT and WASI spectra at 2 m and 10 m bottom depth for  $C_L = 2$  mg/l. The differences can be attributed to Gelbstoff absorption and chlorophyll *a* fluorescence, which is accounted for in HYDROLIGHT but not in WASI. Both sets of spectra were inverted using WASI (eq. 19). During inversion only the bottom depth  $z_B$  was a fitted parameter; and all other parameters were fixed at their correct values. Figure 8B shows the relative errors  $100 \cdot (z_B^{\text{fit}} / z_B - 1)$  as a function of  $z_B$  for  $C_L = 1, 2, 3, 4, 5$  mg/l, where  $z_B^{\text{fit}}$  are the results from inverting the HYDROLIGHT spectra. The influence of the bottom albedo on remote sensing reflectance decreases with increasing depth and increasing concentration of suspended matter. Thus, the accuracy of  $z_B$  determination decreases accordingly. The corresponding errors from inverting the WASI spectra were close to zero and are not shown. Since only  $z_B$  was unknown, the errors in Figure 8B demonstrate the lower limit for model errors. More realistic error estimates are obtained by fitting additional variables such as  $C_0$ ,  $Y$  and  $C_L$  along with  $z_B$ . However, the errors obtained are a mixture of errors from the model and error propagation (see 4.2.4). These two effects can be separated only by performing more detailed studies.

#### 4.2.3 Errors from input data

Each spectrum type has a specific set of input data. Since all input data have uncertainties, it is useful to study the influence of their anticipated errors on the retrieved parameters. Three types of input data can be distinguished: (1) input spectra from a data base, (2) input spectra from actual field measurements, and (3) input parameters. Examples of input data with potentially significant errors are:  $a_i^*(\lambda)$ ,  $a_w(\lambda)$ ,  $b_L(\lambda)$ ,  $a_n(\lambda)$ ,  $t_A(\lambda)$ , and  $t_C(\lambda)$  for type (1);  $L_s(\lambda)$ ,  $E_d(\lambda)$ , and  $R(\lambda)$  for type (2); and  $S$ ,  $b_{b,L}^*$ ,  $b_{b,S}^*$ ,  $\sigma$ ,  $\sigma_L$ ,  $f$ ,  $Q$ ,  $B_n$ , and  $v$  for type (3).

The implications of input data errors on the accuracy of data analysis are studied by simulating measurements using a certain set of input data, and then inverting these simulations with altered input data. The method of altering input data depends on its type: for type (1) other files must be used, for type (2) the input measurements can be simulated, and for type (3) individual parameters have to be changed.

An example is given in Figure 9. Irradiance reflectance was calculated for shallow water using eq. (16). The following water constituent values were used:  $C_0 = 2$   $\mu\text{g/l}$ ,  $C_L = 2$  mg/l,  $Y = 0.3$   $\text{m}^{-1}$ , and  $S = 0.014$   $\text{nm}^{-1}$ . For Figure 9A the wavelength-independent spectrum of bottom albedo,  $a_0(\lambda) = 0.1$ , was chosen. Its absolute value was changed from 0.1 to 0.3 during forward calculation by iterating the parameter  $f_0$  of eq. (22) from 1 to 3, but kept constant at 0.2 during inversion. In this way relative errors of the bottom albedo from -50 % to 100 % were simulated. During inversion only the bottom depth  $z_B$  was a fit parameter. Its relative error is shown in Figure 9A as a function of  $z_B$  and of the relative albedo error. For Figure 9B, the silt spectrum provided with WASI was used as bottom albedo for forward calculation, and the five other bottom types were used during inversion. No fit of the incorrect parameters (areal fractions of the bottom types) was allowed. As expected, the errors depend on the bottom type and decrease with  $z_B$ .

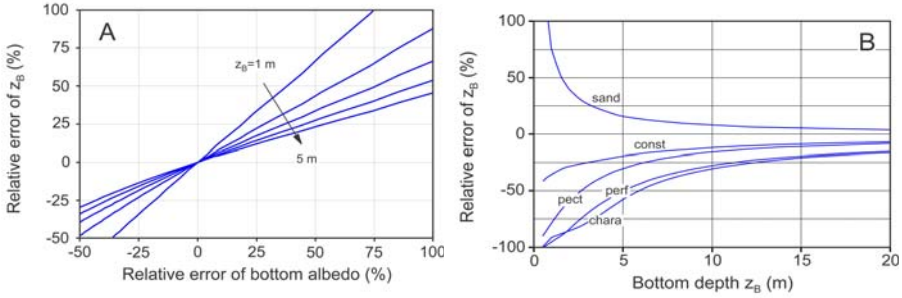


**Figure 9.** Illustration of errors from input data at the example of irradiance reflectance spectra. A: Errors caused by wrong scaling factor of the bottom albedo. B: Errors caused by wrong bottom type.

4.2.4 Error propagation

The influence of an incorrect model parameter value on the accuracy of the fit parameters can be analyzed effectively using the reconstruction mode of WASI, which combines forward and inverse modeling. The parameter of interest is iterated from a low to a high value during forward calculation and kept constant during fitting. With the exception of this parameter, the decision for which parameters to fit and which to fix is made in the same manner as during data analysis. All fixed parameters are kept equal in the forward and inverse mode. When the calculation is started, a series of spectra is calculated and subsequently inverted with well-defined errors for one parameter. A table is generated which lists the values of the iterated parameter, the residuum, the results of all fit parameters, and the relative errors of user-specified parameters.

An example is given in Figure 10. Absorption of water constituents was calculated using eq. (1). During forward calculation, phytoplankton concentration  $C_0$  was changed from 0.5 to 8  $\mu\text{g/l}$ . During inversion  $C_0$  was fixed at 2, 1, and 4  $\mu\text{g/l}$  for curves A, B, and C, respectively. Gelbstoff concentration,  $Y$ , and spectral slope  $S$  were estimated using inversion. Their relative errors are shown as a function of the relative  $C_0$  error. The plots illustrate how  $C_0$  errors induce  $Y$  (Figure 10A) and  $S$  (Figure 10B) errors.

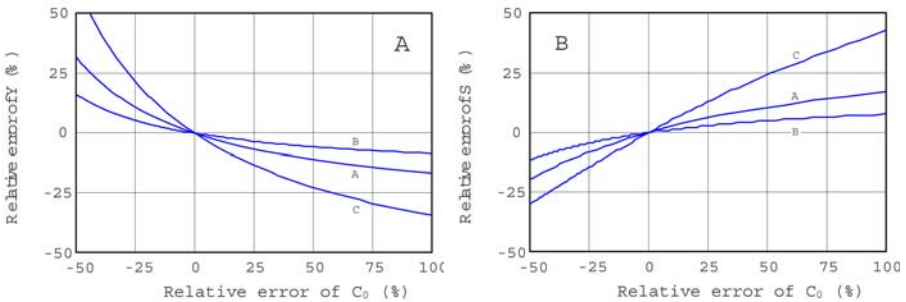


**Figure 10.** Illustration of error propagation at the example of absorption spectra. A: Errors of Gelbstoff concentration  $Y$  caused by  $C_0$  errors. B: Errors of exponent  $S$  of Gelbstoff absorption caused by  $C_0$  errors.

## 5. Conclusions

The Water Colour Simulator WASI is a user-friendly program for forward and inverse modeling of optical *in situ* measurements in aquatic environments. It supports all common types of spectral data obtained from shipborne instruments deployed above and below the water surface. Computationally, the program uses analytic models which are suited for all water types: deep and shallow, inland, coastal, and oceanic. Region-specific optical properties can be accounted for by exchanging the relevant input data.

The main application for WASI is data analysis. WASI is designed to automatically invert large series of spectra in a reasonable time, i.e. on the order of seconds per spectrum. In addition, it is well-suited to analyze errors from different sources by means of simulations. Since a consistent set of models is implemented and the same input data are used for the different spectrum types, data from different instruments can be compared easily (optical closure studies). Vice versa, optical properties of water constituents can be derived indirectly from non-specialized instruments, such as absorption of water constituents from reflectance measurements. Further applications of WASI are visualization of spectral changes upon parameter variation, data simulation, and student training.

WASI does have some restrictions. The implemented models are analytic approximations and do not account for all physical effects, such as fluorescence and Raman scattering or for certain water constituents such as detritus and bubbles. Vertical profiles cannot be calculated, nor can images be processed. Data from instruments on satellite and aircraft cannot be analyzed directly, since no atmospheric model is included. However, the latter can be done indirectly by coupling WASI with such a program.

## 6. Acknowledgements

We are grateful to Nicole Pinnel (Technical University Munich) for providing unpublished measurements of bottom albedo, and to Laurie Richardson (Florida International University) for improving the English of our manuscript.

This work was supported by the German Federal Ministry for Education and Research, Project ID 07 UFE 16/1. It is part of the Special Collaborative Program SFB 454 "Lake Constance" littoral funded by the German Research Foundation DFG.

## 7. References

- Ahn, Y.H., A. Bricaud and A. Morel. 1992. Light backscattering efficiency and related properties of some phytoplankton. *Deep-Sea Research*, 39: 1835-1855.
- Albert, A., and C.D. Mobley. 2003. An analytical model for subsurface irradiance and remote sensing reflectance in deep and shallow case-2 waters. *Optics Express* 11, 2873-2890. <http://www.opticsexpress.org/abstract.cfm?URI=OPEX-11-22-2873>.
- Albert, A. 2004. Inversion technique for optical remote sensing in shallow water. Ph.D. thesis, University of Hamburg. <http://www.sub.uni-hamburg.de/opus/volltexte/2005/2325/>
- Albert, A. and P. Gege. 2005. Inversion of irradiance and remote sensing reflectance in shallow water between 400 and 800 nm for calculations of water and bottom properties. *Applied Optics* (submitted).
- Babin, M., and D. Stramski. 2002. Light absorption by aquatic particles in the near-infrared spectral region. *Limnology and Oceanography*, 47(3), 911-915.
- Bricaud, A., A. Morel and L. Prieur. 1981. Absorption by dissolved organic matter of the sea (yellow substance) in the W and visible domains. *Limnology and Oceanography*, 26: 43-53.
- Buiteveld, H., J.H.M. Hakvoort and M. Donze. 1994. The optical properties of pure water. *Ocean Optics XII*, SPIE, Vol. 2258: 174-183.

- Caceci, M.S. and W.P. Cacheris. 1984. Fitting Curves to Data. *Byte* May 1984: 340-362.
- Carder, K.L., G.R. Harvey and P.B. Ortner 1989. Marine humic and fulvic acids: their effects on remote sensing of ocean chlorophyll. *Limnology and Oceanography*, 34: 68-81.
- Gege, P. 1994. Gewässeranalyse mit passiver Fernerkundung: Ein Modell zur Interpretation optischer Spektralmessungen. Ph.D. thesis, University of Hamburg. DLR-Forschungsbericht 94-15, 171 pp.
- Gege, P. 1995. Water analysis by remote sensing: A model for the interpretation of optical spectral measurements. Technical Translation ESA-TT-1324, 231 pp., July 1995.
- Gege, P. 1998a. Characterization of the phytoplankton in Lake Constance for classification by remote sensing. *Archives fur Hydrobiologia. Special Issues Advances in Limnology*, 53, p. 179-193, Dezember 1998: Lake Constance, Characterization of an Ecosystem in Transition.
- Gege, P. 1998b. Correction of specular reflections at the water surface. *Ocean Optics XIV*, 10-13 Nov. 1998, Kailua-Kona, Hawaii, USA. Conference Papers, Vol. 2.
- Gege, P. 2002a. The Water Colour Simulator WASI. User manual for version 2. DLR Internal Report IB 564-01/02, 60 pp. – The actual version of the manual and of the software can be loaded from the ftp server <ftp.dfd.dlr.de>. Login: *anonymous*, password: *[email address]*, directory: */pub/WASI*.
- Gege, P. 2002b. Error propagation at inversion of irradiance reflectance spectra in case-2 waters. *Ocean Optics XVI Conference*, November 18-22, 2002, Santa Fe, USA.
- Gege, P. 2004. The water colour simulator WASI: An integrating software tool for analysis and simulation of optical in-situ spectra. *Computers and Geosciences*, 30: 523-532
- Gordon, H.R., O.B. Brown and M.M. Jacobs. 1975. Computed Relationships between the Inherent and Apparent Optical Properties of a Flat Homogeneous Ocean. *Applied Optics*, 14: 417-427
- Gordon, H.R. 1989. Can the Lambert-Beer law be applied to the diffuse attenuation coefficient of ocean water? *Limnology and Oceanography*, 34(8): 1389-1409
- Heege, T. 2000. Flugzeuggestützte Fernerkundung von Wasserinhaltsstoffen am Bodensee. Ph.D. thesis, Free University of Berlin. DLR-Forschungsbericht 2000-40, 134 p.
- Kirk, J.T.O. 1984. Dependence of relationship between inherent and apparent optical properties of water on solar altitude. *Limnology and Oceanography*, 29: 350-356.
- Jerlov, N.G. 1976. *Marine Optics*. Elsevier Scientific Publ. Company.
- Jerome, J.H., R.P. Bukata and J.E. Bruton. 1990. Determination of available subsurface light for photochemical and photobiological activity. *Journal for Great Lakes Research*, 16(3): 436-443.
- Mobley, C.D., B. Gentili, H.R. Gordon, Z. Jin, G.W. Kattawar, A. Morel, P. Reinersman, K. Stamnes and R.H. Stavn. 1993. Comparison of numerical models for computing underwater light fields. *Applied Optics*, 32: 7484-7504.
- Mobley, C.D. 1994. *Light and Water*. Academic Press, 592 pp.
- Mobley, C.D. 1999. Estimation of the remote-sensing reflectance from above-surface measurements. *Applied Optics*, 38: 7442-7455.
- Morel, A. 1974. Optical Properties of Pure Water and Pure Sea Water, p. 1-24. In N.G. Jerlov and E. Steemann Nielsen [eds.], *Optical Aspects of Oceanography*. Academic Press London.
- Morel, A. 1980. In water and remote measurements of ocean colour. *Boundary-Layer Meteorology*, 18: 177-201.
- Morel, A. and B. Gentili. 1991. Diffuse reflectance of oceanic waters: its dependence on Sun angle as influenced by the molecular scattering contribution. *Applied Optics*, 30: 4427-4438.
- Mueller, J.L. and R.W. Austin. 1995. Volume 25 of *Ocean Optics Protocols for SeaWiFS Validation*, Revision 1. S.B. Hooker, E.R. Firestone, and J.G. Acker, eds., NASA Tech. Memo. 104566. NASA Goddard Space Flight Center, Greenbelt, Md.
- Nelder, J.A. and R. Mead 1965. A simplex method for function minimization. *Computer Journal* 7:308-313
- Nyquist, G. 1979. Investigation of some optical properties of seawater with special reference to lignin sulfonates and humic substances. Ph.D. thesis. Göteborgs Universitet, 200 pp.
- Pinnel, N. 2005. Spectral discrimination of submerged macrophytes in lakes using hyperspectral remote sensing data. Ph.D. thesis. Limnological Institute of the Technical University Munich (in preparation).
- Preisendorfer, R.W. and C.D. Mobley. 1985. Unpolarized irradiance reflectances and glitter patterns of random capillary waves on lakes and seas, by Monte Carlo simulation. NOAA Tech. Memo. ERL PMEL-63, Pacific Mar. Environ. Lab., Seattle, WA, 141 pp.
- Preisendorfer, R.W. and C.D. Mobley. 1986. Albedos and glitter patterns of a wind-roughened sea surface. *Journal of Physical Oceanography*, 16: 1293-1316.
- Prieur, L. 1976. Transfers radiatifs dans les eaux de mer. Ph.D thesis. Doctorat d'Etat, Univ. Pierre et Marie Curie, Paris, 243 pp.
- Prieur, L. and S. Sathyendranath. 1981. An optical classification of coastal and oceanic waters based on the specific spectral absorption curves of phytoplankton pigments, dissolved organic matter, and other particulate materials. *Limnology and Oceanography*, 26: 671-689.

- Sathyendranath, S. and T. Platt. 1988. Oceanic Primary Production: Estimation by Remote Sensing at Local and Regional Scales. *Science*, 241: 1613-1620.
- Sathyendranath, S., L. Prieur and A. Morel. 1989. A three-component model of ocean colour and its application to remote sensing of phytoplankton pigments in coastal waters. *International Journal of Remote Sensing*, 10: 1373-1394.
- Sathyendranath, S. and T. Platt. 1997. Analytic model of ocean color. *Applied Optics*, 36: 2620-2629.
- Toole, D.A., D.A. Siegel, D.W. Menzies, M. Neumann and R.C. Smith. 2000. Remote-sensing reflectance determinations in the coastal ocean environment: impact of instrumental characteristics and environmental variability. *Applied Optics*, 39(3): 456-469.